NASA Contractor Report 189200

The Development of a Fiber Optic Raman Temperature Measurement System for Rocket Flows

Wim A. de Groot
Sverdrup Technology, Inc.
Lewis Research Center Group
Brook Park, Ohio

July 1992

Prepared for
Lewis Research Center
Under Contract NAS3–25266

National Aeronautics and
Space Administration

The Development of a Fiber Optic Raman Temperature Measurement System for Rocket Flows

Wim A. de Groot*

Sverdrup Technology, Inc.
NASA Lewis Research Center Group
Brookpark, Ohio 44142

Abstract

A fiberoptic Raman diagnostic system for H_2/O_2 rocket flows is currently under development. This system is designed for measurements of temperature and major species concentration in the combustion chamber and part of the nozzle of a 100 Newton thrust rocket currently undergoing tests. This paper describes a measurement system based on the spontaneous Raman scattering phenomenon. An analysis of the principles behind the technique is given. Software is developed to measure temperature and major species concentration by comparing theoretical Raman scattering spectra with experimentally obtained spectra.
Equipment selection and experimental approach are summarized. This experimental effort is part of a program, which is in progress, to evaluate Navier-Stokes based analyses for this class of rockets.

Nomenclature

C	constant representing optical collection efficiency
c	speed of light (2.997×10^{10} cm/sec)
E_{laser}	incident light quantum energy
$E_{s,a-s}$	scattered light quantum energy
h	Planck's constant (6.624×10^{-34} Joule.sec)
I_{laser}	incident light intensity
$I_{s,a-s}$	detected light intensity
N_i	species number density in upper energy level
ΔE	energy difference
λ_{laser}	wavelength of incident light quantum

* Research Engineer, Member AIAA

$\lambda_{s,a-s}$ wavelength of Stokes/anti-Stokes scattered quantum
ν_i Raman shift
Ω solid angle of detection
$\sigma_{s,a-s}$ Raman scattering cross-section

Introduction

The application of advanced experimental diagnostics in efforts to gain insight into the inner workings of rocket engines has not kept pace with computational fluid dynamics (CFD) code predictions. While many advanced experimental methods have been used in airbreathing engines, not much work has been done utilizing these methods to quantify fluid dynamic and thermodynamic variables inside rocket engines. The result is that, for the design of new rockets,engineers rely on flow predictions with little experimental data on local, internal flow phenomena.

Current rocket design efforts are based on the JANNAF-TDK methodology[1] in conjunction with global prototype performance parameters. In this methodology, the combustion chamber is divided into zones, each zone having a fixed mixture ratio. A one dimensional kinetics code (ODK) calculates how the combustion process inside each zone proceeds towards the throat. For medium and large size rockets an empirical methodology is used to calculate mixture ratios and mass flows in each zone. Energy losses caused by incomplete combustion are represented by a combustion efficiency which is determined empirically. The physics of small rockets, however, causes the application of this methodology to small rockets to be less appropriate.
The large surface to volume ratio in small rockets causes wall effects, such as heat flux to the wall, to be much more dominant than in larger rockets. As opposed to large scale rockets, shear layer mixing and boundary layer effects in small rockets govern a large section of the flowfield. As a consequence, the effects of severe gradients are much more important in the analysis of small rocket chambers.

The JANNAF-TDK methodology uses the two dimensional kinetics (TDK) method of characteristics (MOC) to calculate the flow through the exhaust nozzle. The MOC is an inviscid scheme for calculating the flow properties of reacting gas mixtures. Thrust losses due to viscous effects in the boundary layer are estimated in a separate module. For large and medium size rockets, where boundary layers are a minor part of the flowfield, this approach produces excellent results. For small rockets, however, the boundary layers are a dominant part of the nozzle flow. Because of this, the use of an inviscid code on this type of device is less appropriate.

With respect to modeling, therefore, small rockets pose a significantly different and more complex situation than large rockets. For these reasons, Navier-Stokes based analyses of small rockets have been undertaken. Direct experimental verifications of code predictions for local chemistry and fluid dynamic parameters, however, have not been made to date. In large part this lack of experimental data on local flow properties is due to the fact that the chemically reacting flow environments are intrinsically hostile, especially under the high pressure conditions inherent to rocket engines. The advent of powerful laser sources and other new optical tools, such as fiber optics and diode array detectors, has opened up a whole new world of diagnostics methods to analyze the types of physical processes of interest. Drake et al.[2] measured temperature and concentration fluctuations in a turbulent diffusion flame using Raman scattering. Seasholtz et.al.[3] made use of the Doppler shift and Doppler broadening of a single mode laser beam to measure velocity and temperature in a H_2/O_2 rocket plume. And Barlow et al.[4] used a combination of spontaneous Raman scattering, Rayleigh scattering and laser induced fluorescence (LIF) to determine the chemical structure and the spatial structure of reactions zones in highly turbulent, methane jet flames. To monitor chemical systems in remote or hostile environments, Weyer et. al.[5] described a fiber optics based spectroscopic system. To the authors knowledge, however, fiber optic technology has not yet been coupled with non-intrusive diagnostics in rocket combustion chambers.

Modern, non-intrusive optical diagnostics can be used to gain insight into the physical processes important to the operation of the thruster. Different types of diagnostics are available to detect many of the reactive fluid flow parameters. The advantages and disadvantages of applying spontaneous Raman scattering to different combustion phenomena are described in sufficient detail elsewhere[6,7]. The low level of luminosity in hydrogen-oxygen flames makes the use of spontaneous Raman scattering, which is a few orders of magnitude weaker than other scattering processes such as Rayleigh scattering, feasible. The Raman spectrum of each species provides a unique fingerprint that is concentration and temperature dependent and is, therefore, a promising diagnostic tool in the analysis of temperature and species. Due to the signal intensity limit, the technique is limited to the measurement of major species ($N>\sim10^{18}$ cm^{-3}) only.

In previous applications of Raman scattering, see, for example, Ref.8, the experiments have been designed to accommodate the technique. Choices of unconfined flames in a clean laboratory environment facilitate these applications. This paper describes the application of a spontaneous Raman scattering technique for the measurement of species concentration and temperature in 100 N-class, H_2/O_2 rocket engines chambers currently being tested in a rocket test facility[9]. This class of rockets was designed for

space station reboost and stabilization. The I_{sp} of these rockets is approximately 345 sec for a O/H mass mixture ratio of 8 (stoichiometric). Software has been developed and described here that can be used iteratively with experimental data to obtain the temperature and major species number density. This is followed by a description of the design of the experimental apparatus.

Theory

Extensive theoretical explanations of the physics leading to the Raman effect are given elsewhere[10]. A straightforward explanation will be given based on quantum theoretical considerations.

Diatomic Species: Figure 1 shows an energy level diagram of a diatomic molecule. The discrete rotational and vibrational energy levels are indicated by the quantum numbers J and v, respectively. These levels are unique for each type of molecule and depend on molecular properties, such as the mass of the nuclei, the separation between the nuclei (moment of inertia), and on the forces inside the molecule (centrifugal forces, interaction between the different angular momenta in the molecule). A molecule that resides in a certain energy level is specified by the quantum numbers denoting this level. When this molecule collides with an incident light quantum (or photon) with energy equal to $h\nu_{laser}$, the light can be scattered without a change in energy (Rayleigh scattering), or after an exchange of energy with the scattering molecule (Raman scattering). The energy exchanged in the Raman scattering process can only be equal to the energy differences between two stable rovibronic molecular energy levels. Quantum mechanical considerations[11] lead to specific selection (or transition) rules, so only certain transitions are allowed. Transitions between vibrational levels must occur between adjacent vibrational levels (i.e. $\Delta v=\pm 1$). Transitions between rotational levels must occur between alternate rotational levels (i.e. $\Delta J=0,\pm 2$). The process in which a molecule absorbs energy from the incident photon, thus leaving the molecule in a higher excited state and the photon less energetic is termed Raman Stokes scattering. When a molecule relinquishes energy to the photon, it transitions to a lower molecular energy level, leaving the scattered photon more energetic. This is referred to as Raman anti-Stokes scattering. At ambient temperatures, all but an insignificant fraction of the molecules reside in the vibrational groundstate, the lowest allowable energy level. Anti-Stokes scattering, therefore, will be a very weak process. As the temperature increases this process becomes increasingly important.

Since the Raman effect is a scattering process instead of an absorption-emission process, such as LIF, it has two distinguishing features. First, the incident light quantum does not have to match the separation in energy between two molecular energy states to initiate Raman scattering(if it does match, the

process is referred to as resonance Raman scattering). Second, the timescale of Raman scattering is negligible (< 10^{-14} sec in the visible spectrum). This means that practically no collisional or other quenching is possible, a phenomenon which makes LIF results difficult to interpret in some cases.

Figure 1 provides a graphic description of the processes described above. In this figure, the combined energy of the scattering system (molecule and light quantum) at the time of collision is indicated by the upper dashed line, a virtual state of the molecule. For Raman scattering, the scattered photon can possess energy E_{Stokes} or $E_{a-Stokes}$. In equation form this is:

$$E_{S,a-S} = E_{laser} \mp \Delta E_{mol} \qquad (1)$$

This can be related to the wavelength of the photon as:

$$\frac{1}{\lambda_{S,a-S}} = \frac{1}{\lambda_{laser}} + \frac{\Delta E_{mol}}{h.c} \qquad (2)$$

Because the wavelength of the scattered light is dependent on the difference between two adjacent energy levels of the scatterer , the signal is species specific. The characteristic Raman shift, given by the second term on the right hand side of equation 2, is independent of the wavelength of the incident light. It is expressed in wavenumbers ν_i. The Raman shift for species relevant to H_2/O_2 combustion are tabulated in Table I. Detection of scattered light at a wavelength determined by the scatterer and incident light quantum indicates the presence of that species. The intensity of the scattered light is given by[12]:

$$I_{S,a-S} = C \cdot \Omega \cdot I_{laser} \cdot (d\sigma_{S,a-S}/d\Omega) \cdot N_i \qquad (3)$$

Here the differential scattering cross section $d\sigma_{s,a-s}/d\Omega$ is used as only a finite solid angle Ω is experimentally obtained. The Raman scattering cross section $\sigma_{s,a-s}$ represents the probability that a molecular energy transition occurs due to a collision and indicates the resultant amount of light scattered over the full solid angle of 4π steradian. This parameter depends on the energy of the incident light quanta (wavelength of light) and the polarization of the incident and scattered light. Values of $d\sigma_{s,a-s}/d\Omega$ have been measured for a number of species[13] and are tabulated for the species of interest in Table I. These are

values for which the incident and scattered light are polarized perpendicular to the scattering plane. Corrections to account for unpolarized incident and scattered light are given elsewhere[14]. Assuming thermal equilibrium, the number density of a given species in each energy level depends on the total species number density and the temperature. N_i can be calculated using the Boltzmann distribution. The constant C is used to account for the efficiency of the detection optics.

Triatomic Species: Water (H_2O) is the major combustion product and is a triatomic species. As such, the energy levels are more complicated than with diatomic molecules. Three vibrations must be specified by their vibrational quantum numbers v_1, v_2, and v_3. Rotationally, H_2O can be approximated as an asymmetric top molecule. An additional complication occurs, however, due to the interaction between the electronic motion and the rotation. This causes each possible rotational energy level with quantum number J to be split into 2J+1 possible rotational energy levels with the same rotational quantum number but slightly different energy levels. The exact calculation of these energy levels have been given elsewhere[15,16].

The fundamental scattering phenomenon for H_2O is the same as for diatomic molecules. This means a vibrational selection (transition) rule of $\Delta v_1=\pm1$, $\Delta v_2=\pm1$, or $\Delta v_3=\pm1$. The rotational selection rules within each vibrational transition are $\Delta J=0,\pm1,\pm2$[15]. Additional selection rules that govern transitions between the split rotational levels are given in the same reference. The probability that an energy exchange occurs during a collision of a water molecule with a light quantum depends on which of the three vibrational quanta v_1, v_2, or v_3 is the exchange partner. Analogous to diatomic molecules, this probability is given by a Raman scattering cross section. For two of these vibrations, the cross sections have been measured (Table I). The third transition is extremely weak and has never been measured.

The wavelength of the light scattered by H_2O molecules can be calculated using Equation 2. The intensity of this light, given specific experimental conditions, can be calculated from Equation 3. The number densities N_i can then be calculated using the Boltzman distribution for a given temperature.

Discussion

A number of different approaches to using spontaneous Raman scattering for temperature measurements have been taken. Wu et al.[17] measured the temperature using an integrated Raman Stokes line intensity method with nitrogen and assumed that the presence of other species could be neglected. The results were then validated by comparing temperature measurements in a calibration flame taken with the Raman method to the temperature measurements

taken with a thermocouple. An integrated line method was used by Dibble to measure all species present[8]. This removes some uncertainty but greatly complicates the experiment. Temperature can also be measured by comparing the Stokes against the anti-Stokes line intensities directly. This line ratio method has been described elsewhere[12], and the temperature is determined from:

$$\frac{I_S}{I_{a-S}} = \frac{(\nu'_{laser}-\nu')^4}{(\nu'_{laser}+\nu')^4} \exp\left(\frac{hc\nu}{kT}\right) \qquad (4)$$

At low to moderately high temperatures, the weakness of the anti-Stokes line make the application of this technique difficult. For the analysis of small rocket engines, therefore, a technique in which the shape of the rotational distribution is used to measure the temperature has been selected. This technique avoids problems related to low light intensity and multiple species.

Predictions

Software has been written to extract temperature and species information by comparing experimental and theoretical spectra. For an initial calculation of a spectrum, information is needed a priori about the temperature and species number density. As with any iterative procedure, good initial inputs will lessen computational requirements. At each location in the combustion chamber, approximations for the initial temperature and number densities can be obtained from the zonal ODK model described earlier. Calculations of this complexity are not required, however, and to simplify the analysis, a six equation chemical equilibrium scheme was written involving the six major equilibrium reactions for H_2/O_2 combustion, to predict equilibrium species fractions and temperature from a given input mixture ratio and injection temperature. For example, close to the injector, the injector mixture ratio, which is oxygen rich, can be assumed. Further down the combustion chamber, the overall mixture ratio can be assumed. And near the wall inside the hydrogen film, the assumption of equilibrium with the wall is justified. Thus, the prediction allows calculation or manual input of the initial assumption on temperature and species fraction.

With the temperature thus calculated or assumed and assuming local thermal equilibrium, the species distribution over all possible energy states can be calculated using the Boltzmann distribution. All possible rovibronic energy states are obtained using Herzberg constants[11,15]. Interaction between electronic motion and rotation[11,15] causes a slight shift in these levels, which is included. Substitution of these energy values and the

assumed temperature into the Boltzmann distribution provides the probability distribution of the molecules over the energy states. For some relevant molecules H_2, O_2, N_2, OH, these calculated distributions are shown for three different temperatures in figure 2a,b, and c. Nitrogen is included because it is the best documented Raman spectrum and so can be used for calibration purposes. Ortho and para modifications of the homogeneous molecules H_2, O_2 and N_2[11] cause the distribution over the odd and even J rotational levels to be 3:1, 1:0, and 1:2 respectively. The split of the rotational J levels of H_2O due to the interaction of electronic motion with rotation[16] gives (2J+1) rotational sublevels for each J, indicated by the subscript τ. Figure 3 shows the rotational distribution of one vibrational level, the $v_1=0$, $v_2=0$, $v_3=0$ level, for water at a temperature of 298 K.

Using these energy levels, the selection rules given[11] and the wavelength of the incident photon, the spectral locations of the Raman scattered light from molecules residing in any energy level are calculated from Equation 2. The calculated number density in each level, together with the laser intensity I_{laser} and the tabulated scattering cross-section factor provide the scattered intensity at these spectral locations. A correction has been introduced to account for the fact that the incident light and scattered light are unpolarized[14]. The spectral shape of each line is approximated by a Lorentzian profile. The optical efficiency factor C is experimentally determined. The solid angle Ω over which light is detected is an optical design parameter. It depends on the f# of the collection lens and can be calculated. With these parameters, the emitted intensity is calculated from Equation 3. Combining the spectral location and intensity results yields an accurate prediction of the measured spectrum. Figure 4 shows a prediction of the Raman Stokes Q-branch (where Q-branch denotes $\Delta v=+1$, $\Delta J=0$) of oxygen for three different temperatures. Two effects cause the individual rotational lines to merge: the laser linewidth, and the resolution (instrument function) of the detector. The finite linewidth of the incident laser is incorporated in the calculations by representing the laser linewidth as a Gaussian probability distribution of photons over the wavelengths covered by the laser emission. The Lorentzian profile of each transition is convoluted with the laser distribution. Variables in the calculation are the laser wavelength, power, and bandwidth, represented by the full width at half maximum (FWHM). As the instrument resolution has not been measured to date, an assumed instrument function has been included.

The theoretical spectra can then be compared to measured spectra in an iterative procedure applied to obtain temperature and species densities estimates. Software has been written to do this. The software can be run both in batch mode or interactively. In the batch mode a section of the spectrum that

has been measured is compared by means of a least squares fit method with an initial prediction, based on assumed temperature and species data. An unacceptable fit generates a new set of assumed data, with which a second spectral prediction is made, leading to a new least squares fit comparison. In this way, a best fit can be obtained. The temperature and species data that have been used to calculate the best fit prediction are a good estimate of the experimental conditions. Due to the large number of variables, this iterative procedure can be prohibitively long. The interactive procedure is faster. Here, a spectral prediction is made and compared graphically with the experimental result. Based on this comparison, a refined estimate can be made to set the values for the temperature and species.

To test the code, predictions were compared against experimental results reported by Rakestraw et.al.[18]. In that work, coherent anti-Stokes spectra (CARS) of nitrogen in air at ambient conditions and at T=2310 K, P=16 atm. were measured by means of a linear array and an unintensified charge-coupled device (CCD) camera. Since the CCD provides more detail, these measured spectra were used to compare against predictions. The CARS signal scales quadratically with density whereas the spontaneous Raman scattering signal scales linearly with density. The intensity value of the prediction was therefore compared against the square root of the CARS intensity. The spectra were normalized with respect to the peak value. To facilitate the comparison, a small vertical offset was added to the prediction to account for the read noise of the CCD. Comparisons of experimental and calculated data are shown in figure 5a and b. In these figures, the predictions (dotted line) are projected onto experimental results (solid curve). The predictions for ambient conditions give an excellent match, except for the location of the bandhead which is slightly shifted. Since temperature information is extracted from the shape of the rotational distribution, the comparison shows that an accurate determination is possible. Some of the discrepancies can be attributed to the lack of knowledge on the experimental details and instrument function, which were accounted for in the prediction. The discrepancy at the band head is probably due to the constructive/destructive interference effects in the CARS technique, which is caused by overlapping transitions of closely spaced lines[19].

In the high temperature, high pressure case, however, a greater difference was observed. Again, the location of the bandhead is slightly shifted, but this time, the magnitude is also underpredicted. Furthermore, the second vibrational band (from v=1 to v=2) shows a large discrepancy in magnitude. In this case the discrepancies at the band head can be attributed to collisional narrowing caused by high pressure, which affects both the CARS and the spontaneous Raman signal at higher pressures[19], but which to date has not been accounted for in the prediction. Constructive/destructive interference effects in the CARS

technique, caused by overlapping transitions of closely spaced lines will affect the second vibrational transition, where rotational lines of the first and second transition overlap. Still, accurate temperature measurements can be extracted from the total shape of the rotational distribution in the first vibrational transition, and excellent agreement with experimental results was obtained.

Experimental Philosophy

In an oxygen rich combustion zone, such as in the combustion chamber core region, oxygen spectra can be used to obtain estimates of the temperature and oxygen number density. Figure 1 shows that in general, for all species, the energy difference between vibrational states is significantly larger then between rotational states. The rotational states contribute only to the minor details. The energy difference between the two lowest vibrational states of oxygen is approximately 3.1×10^{-13} ergs. This can be translated into a Raman shift for oxygen of 1556 cm^{-1}. Incident laser light with a frequency of 590 nm. gives, according to Equation 2, scattered light at a spectral location of 649.6 nm. Measuring this scattered light around that location yields an experimental spectrum to compare against the theoretical spectrum. Figure 4 shows these theoretical spectra of oxygen for three different temperatures. The slope of the curve on the left side represents the rotational distribution, which is a measure of the temperature. The temperature can be extracted by fitting the theoretical to the experimental spectra.

In zones where H_2O is the major species, such as in the region ahead of the throat, there are three Raman shifts, each corresponding to one vibrational sequence. Only one transition probability (scattering cross section), however, is strong enough to yield a useful signal. The Raman shift caused by this transition is 3652 cm^{-1}. For an incident laser wavelength of 590 nm., Raman spectra for water will be strongest around 752.5 nm. Examples of these spectra calculated for three temperatures are give in Figure 6. At higher temperatures, the H_2O molecules will be distributed over many possible energy states. Because of this, the final spectrum is smeared over a wide spectral range, causing the signal to become weak, and significant details to disappear. The impact of this smearing on the results has not been determined as yet.

Experimental

The Raman scattering system described in this section will be used to measure temperature and species in low thrust H/O rocket as described in Ref. 9. The 100 N. class rockets have a chamber volume of approximately 10 cm^2, operate at a chamber pressure of

around 0.65 MPa, and span a range of mixture ratios from 6 to 8. Accessibility to this axisymmetric rocket is extremely difficult. The use of fiber optics, in combination with water cooling and shrouding with nitrogen or hydrogen is being studied. As an intermediate step to verify the feasibility of Raman scattering diagnostics in the combustion environment of a 0.65 MPa, H_2/O_2 combustion chamber, a two dimensional rocket is being built[20]. The design of this rocket allows the injector of one of the axisymmetric rockets to be installed and uses quartz or fused silica windows, shrouded with nitrogen, to provide the required optical access. Figure 7 shows a schematic of the 2-D chamber. This chamber should provide a close approximation of conditions in a real rocket.

The signal strength of Raman scattering is three or more orders of magnitude weaker than other molecular scattering processes, such as Rayleigh scattering. Therefore, practical applications of the Raman technique require the design of an experiment in which each component has been designed or selected for optimum performance.

A flashlamp-pumped dye laser is used as the source of incident light. The lasing medium is a Rhodamine dye dissolved in ethylene glycol. Rhodamine was chosen for its high energy output, long lifetime, and optimal wavelength. The laser pulse length is of the order of 2.5 μsec with a maximum pulse rate of 10 Hz. There is a tradeoff between high laser energy output, which is desirable to enhance the Raman effect, and a narrow laser bandwidth which is desirable to resolve the rotational details. Laser specifications are given in Table II. Phenomena that could interfere with the Raman technique are fluorescence, multi-photon excitation, dissociation, or ionization. To minimize these, a longer laser pulse length has been chosen to distribute the energy with a lower average intensity.

The use of high energy pulsed lasers requires the careful design and selection of optics. Two breakdown mechanisms of optical components as the consequence of high energy density exposure are common: the breakdown of the electric field of the optical material, and the thermal breakdown due to local "hot spots" which are caused by focused laser light. Optical components made of high quality fused silica often have a damage threshold of 10^9 W/cm^2. A careful design of the optical system, based on this limit is necessary. This does not, however, account for dust accumulating on optical surfaces. To prevent damage due to contamination, the laser and optical system has been housed in a clean room.

Optical fibers are used to guide the incident light and detected light. This eliminates alignment problems and light scattering problems that are inherent in the test environment. Two 1000 μm diameter fibers with "hi-power" SMA-905 connectors and a NA

(Numerical Aperture) of 0.22 (an acceptance angle of 25.4°) were selected. Ceramic connectors with no epoxy near the tip were used. Fibers with metal connectors and epoxy at the tip were tested, but cracked at the fiber surface. The selection of these optical fibers was straightforward. To retain desired beam properties of the probe beam, a single mode fiber should ideally be used. However, single mode fibers are not compatible with the maximum beam energy that must be transmitted. Additionally, for compactness and flexibility, a minimum diameter fiber should be used. To improve spatial resolution, reduction of the probe volume is required which can be accomplished by a reduction in the fiber diameter. A tradeoff between this and the power density limit led to the choice of fiber.

The 6 mm diameter laser beam is coupled into the fiber by means of a high power microscope objective (magnification of 5x). The focal point of the laser beam is placed ahead of the fiber entrance, such that the beam is expanding and has a diameter of about 800 μm at the fiber entrance. This practice prevents local "hot-spots" from occurring inside the fiber. Measurements have shown that slightly more then 70 % of the laser energy is coupled through the fiber. The exit of the fiber, as well as the refocusing lens are purged with clean dry air to prevent dust from settling on the surfaces. The refocusing lens is a best-fit bi-convex lens of f#1.0 (diameter 25.4 mm, fl 25.4 mm), the choice being limited by space constrictions. This lens creates a focused image (making up the probe volume) of 1000 μm diameter. The collection system has an effective f# of 2.0, and consists of a collection lens, two baffles to reduce stray light, a Raman notch filter, and a set of collimating and refocusing lenses. This system collects Raman scattered light from the probe volume and focuses it into another 1000 μm diameter fiber.

The design of the receiving system is such that the image of the receiving fiber on the probe volume is about 1 mm diameter, causing an effective probe volume of roughly 0.5 mm^3. The collected light is transmitted back to the clean room, where it is coupled into a triple spectrometer for stray light rejection. A lens of diameter 25 mm and focal length 40 mm is used to refocus the light exiting the fiber and to match the f#6.3 of the spectrometer. The spectrometer resolution is 0.035 nm with a 1200 grating, 0.023 nm with a 1800 grating, and 0.016 to 0.019 (depending on the wavelength) with a 2400 grating. Based on grating efficiencies given for the master gratings, the throughput varies from ~5% at 700 nm to ~12% at 500 nm. The spectrometer projects a selected part of the spectrum on a red enhanced, intensified linear diode array with 700 diode elements, which is mounted onto the exit plane of the spectrometer. The array is gated to minimize dark current. The gating coincides with the arrival of the scattered light on the photosensitive surface. The length of the gate pulse is selected to cover the entire scattered pulse. Equipment time delays and light

propagation times differ from nanoseconds to microseconds. A 400 MHz oscilloscope is used to verify that both pulses coincide. The experimental schematic is given in figure 8a and the timing diagram is shown in figure 8b. A command from the computer to the array controller initiates the measurement sequence. The controller triggers the dye laser, which emits a laser pulse after some delay. The laser triggers the gate pulser, which opens the gated array after another delay. The light detected by the array is read by the controller and the measured spectrum is stored in a computer. These spectra are downloaded on a VAX mainframe.

An order of magnitude calculation based on the above described experimental system will give an idea of the feasibility of current approach. To date, 800 mJ pulses have been successfully coupled into the fiber, with a coupling efficiency of roughly 70%. This gives an energy of 560 mJ in the probevolume, translating into approximately $1.7*10^{18}$ photons at 590 nm. The nitrogen number density in air at ambient conditions is approx. $2.5*10^{19}$ molecules/cm^3. The differential Raman scattering cross section of the Q-branch of nitrogen is $2.31*10^{-31}$ cm^2/sr. The f#2.0 of the collecting lens translates into a solid angle of collection of 0.43 sr. The section of the laser beam imaged is about 1 mm. Assuming an optical efficiency of 95% for the anti-reflection coated lenses, this means that about $3.2*10^5$ photons enter the spectrometer. If an efficiency of 6% at 680 nm (the wavelength of radiation of the Raman Stokes Q-branch under excitation of a laser wavelength of 590 nm) is assumed, about $1.9*10^4$ photons reach the exit plane. An installed grating of 1800 spreads the Q-branch of nitrogen over about 35 diodes, providing an average number of photons per diode of 550. This satisfies the detection criteria determined by the array, so the technique is feasible.

Additional gains in signal level can be obtained by improving the laser-fiber coupling and the energy output of the laser, which can be done by changing the dye concentration. In cases where stray light will not be a concern (away from the incident laser line), a simpler spectrometer will suffice, improving the throughput and consequently the signal.
Currently, the experimental effort is in the development stage, and signals have not yet been obtained.

Summary

An order of magnitude analysis has shown the feasibility of the use of spontaneous Raman scattering to measure temperature in a H_2/O_2 rocket. An analysis of Raman scattering has been used to develop a software package to predict Raman spectra based on temperature and species. This software allows the user to interactively change the temperature and species to achieve best fit between experimental results and analysis, leading to a

determination of the experimental temperature. To test the validity of this approach, experimentally obtained spectra found in literature[18] were compared with predicted spectra with good agreement.

The design of a fiber optic based Raman scattering system to generate the experimental spectra is described. The use of fiber optics proved to be convenient during calibration and testing.

References

[1] "JANNAF Rocket Engine Performance Prediction and Calculation Manual", CPIA Publication 246, April 1975.

[2] Drake, M.C., Lapp, M., Penney, C.M., Warshaw, S. and Gerhold, B.W.:"Measurements of Temperature and Concentration Fluctuations in Turbulent Diffusion Flames using Pulsed Raman Spectroscopy" Eighteenth Symposium (International) on Combustion, The Combustion Institute, Pittsburgh, 1981, pp. 1521-1531.

[3] Seasholtz, R.G., Zupanc, F.J. and Schneider, S.J.: "Spectrally Resolved Rayleigh Scattering Diagnostic for Hydrogen-Oxygen Rocket Plume Studies" AIAA 29th Aerospace Sciences Meeting, January 7-10, Reno, Nevada, 1991.

[4] Barlow, R.S., Dibble, R.W., Starner, S.H., Bilger, R.W., Fourguette, D.C. and Long, M.B.:"Reaction Zone Structure in Dilute Methane Jet Flames Near Extinction" AIAA 28th Aerospace Sciences Meeting, January 8-11, Reno, Nevada, 1990.

[5] Weyer, L.G., Becker, K.J. and Leach, H.B.:"Remote Sensing Fiber Optic Probe NIR Spectroscopy Coupled With Chemometric Data Treatment", Applied Spectroscopy, Vol. 41, No. 5, 1987, pp. 786-790.

[6] Lapp, M. and Penney, C.M.,"Raman Measurements on Flames", From *Advances in Infrared and Raman Spectroscopy* (R.J.H. Clark and R.E. Hester, Ed.), Chapt. 6, Heyden, London, 1977.

[7] Lapp, M., "Raman-Scattering Measurements of Combustion Properties", From *Laser Probes for Combustion Chemistry* (D.R. Crosley, Ed.), Amer. Chem. Soc. Symp. Series, Vol. 134, Chapt. 17, 1980.

[8] Dibble, R.W., Kollmann, W., and Schefer, R.W."Conserved Scalar Fluxes Measured in a Turbulent Nonpremixed Flame by Combined Laser Doppler Velocimetry and Laser Raman Scattering", Combust. Flame, Vol. 55, pp. 307-321, 1984.

[9] Arrington, L.A. and Schneider, S.J.,"Low Thrust Rocket Test Facility", 26th JPC conference, Orlando, Florida, 1990, AIAA Paper 90-2503.

[10] Placzek, G.,"Rayleigh-Streuung und Raman-Effekt", from *Handbuch der Radiologie*, Vol. VI, (E. Marx, Ed.), Akademische Verlagsgesellschaft, Leipzig, 1934.

[11] Herzberg, G.,"Molecular Spectra and Molecular Structure I", pp. 121, 2nd Ed., Reprint 1989, Krieger Pub. Co.

[12] Lederman, S.,"The use of Laser Raman Diagnostics in Flow Fields and Combustion", Prog. Energy Combust. Sci., Vol.3, pp 1-34, 1977.

[13] Schroetter, H.W. and Kloeckner, H.W.,"Raman Scattering Cross Sections in Gases and Liquids" From *Raman Spectroscopy of Gases and Liquids* (A. Weber, Ed.) Topics in Current Physics: Springer Verlag, 1979.

[14] Hirschfeld, T.,"Correction of Raman Cross Section from Laboratory to Remote Spectrometer Geometries", Applied Spectroscopy, Vol. 27, No. 5, 1973.

[15] Herzberg, G.,"Molecular Spectra and Molecular Structure II", pp. 489, 2nd Ed., Reprint 1991, Krieger Pub. Co.

[16] Wang, S.C.," On the Asymmetrical Top in Quantum Mechanics", Phys. Rev. Vol. 34, pp. 243, 1929.

[17] Wu, M.Z., Walterick, R.E., de Groot, W.A., Jagoda, J.I., Strahle, W.C.:"Turbulent Diffusion Flame Properties Behind a Step", AIAA 29th Aerospace Sciences Meeting, Reno, Nevada, January 7-10, 1991.

[18] Rakestraw, D.J., Lucht, R.P., and Dreier, T.,"Use of a charge-coupled device camera for broadband coherent anti-Stokes Raman scattering measurements", Applied Optics, Vol. 28, No.19, 1989.

[19] Eckbreth, A. C.,"Laser Diagnostics for Combustion Temperature and Species", Energy and Engineering Science Series, Vol. 7, Abacus Press, 1988.

[20] Reed, B.D., Biaglow, J.A.; Private Communication.

Table I. Raman Shifts and Differential Raman Scattering Cross Sections for Some Relevant Species (from Ref. 13).

Species	Raman Shift ν_j (cm^{-1})	$(d\sigma_{s,a-s}/d\Omega) * (1/\lambda_{laser}-\nu_j)^{-4}$ (cm^6/sr)
N_2	2330	$5.05*10^{-48}$
H_2	4160	$18.2*10^{-48}$
O_2	1556	$4.55*10^{-48}$
OH	3570	
H_2O	3652 1595 3756	$17.2*10^{-48}$ $0.04*10^{-48}$

Table II. Laser Properties for Rhodamine dye (590 nm.)

Energy Output per pulse (Joule)	Bandwidth FWHM (nm.)
2.0	Broadband
1.0	0.03
0.6	0.003

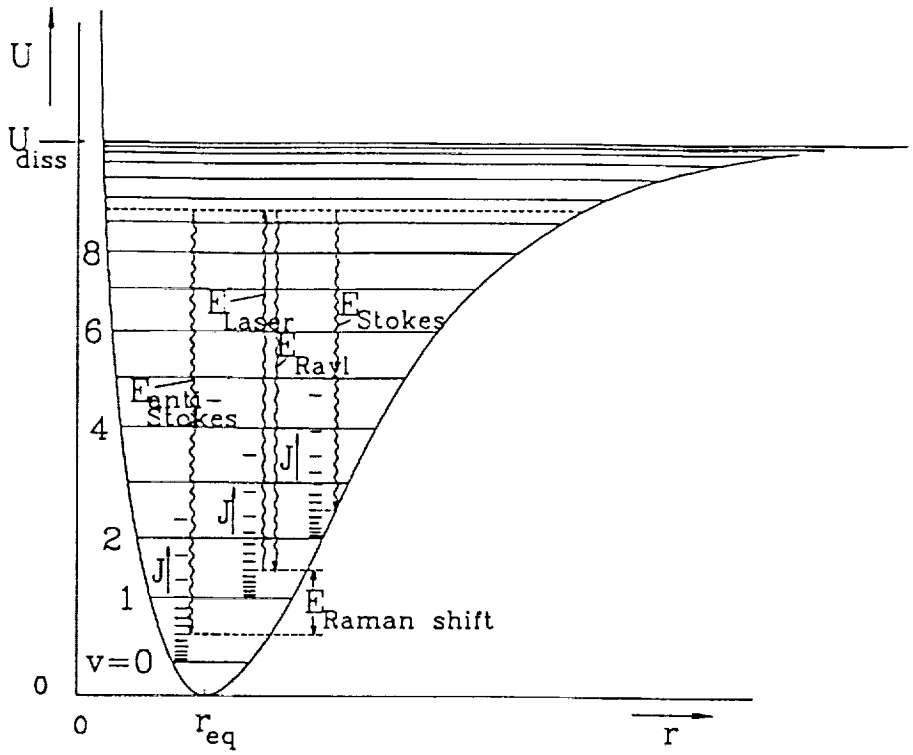

Figure 1. Raman Scattering Energy Principle.

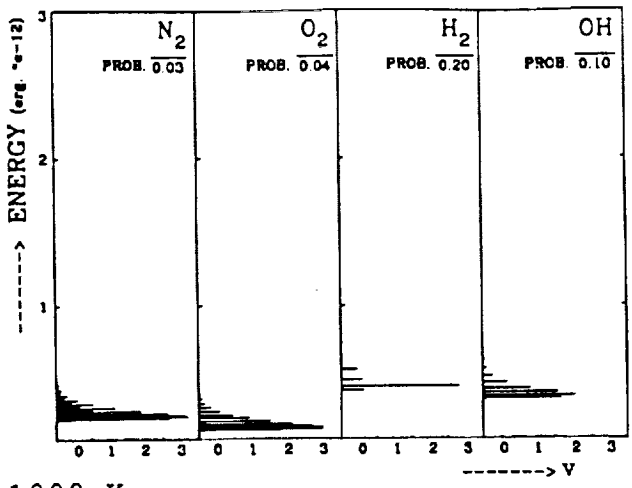

a. T=1000 K.

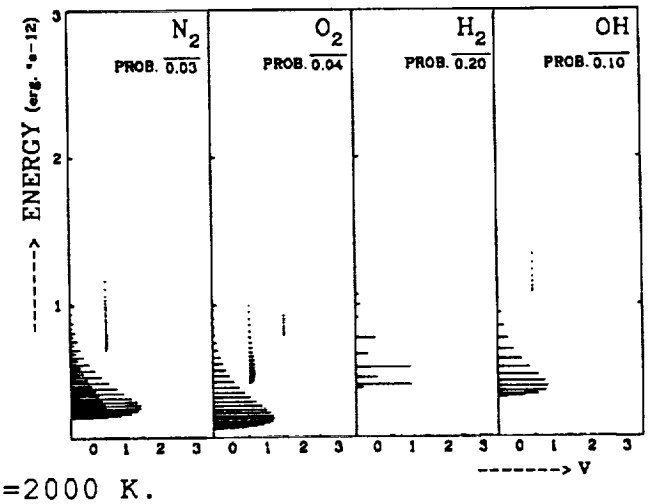

b. T=2000 K.

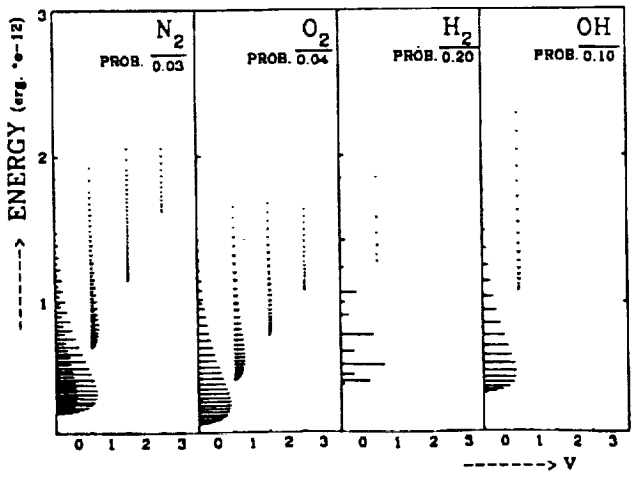

c. T=3000 K.

Figure 2. Molecular distribution over the energy levels for four diatomic molecules at three different temperatures.

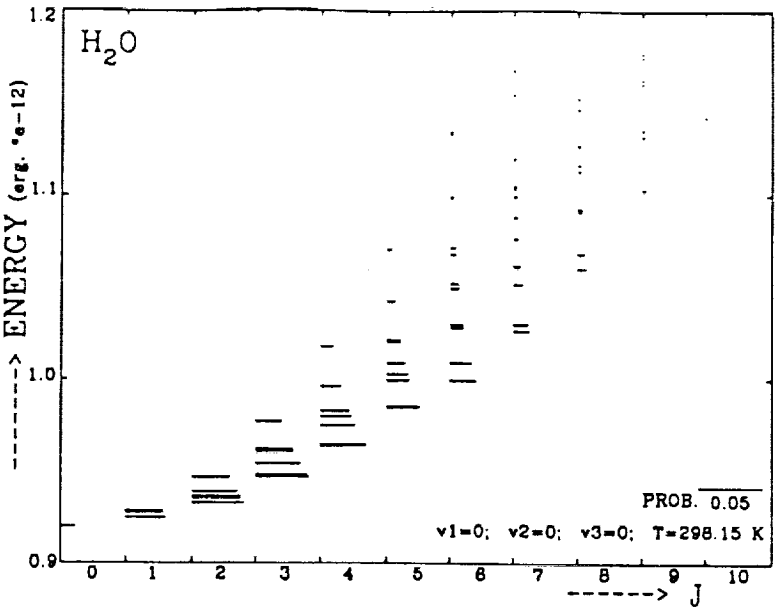

Figure 3. Molecular distribution over the energy levels for water in the vibrational groundstate at T = 298 K.

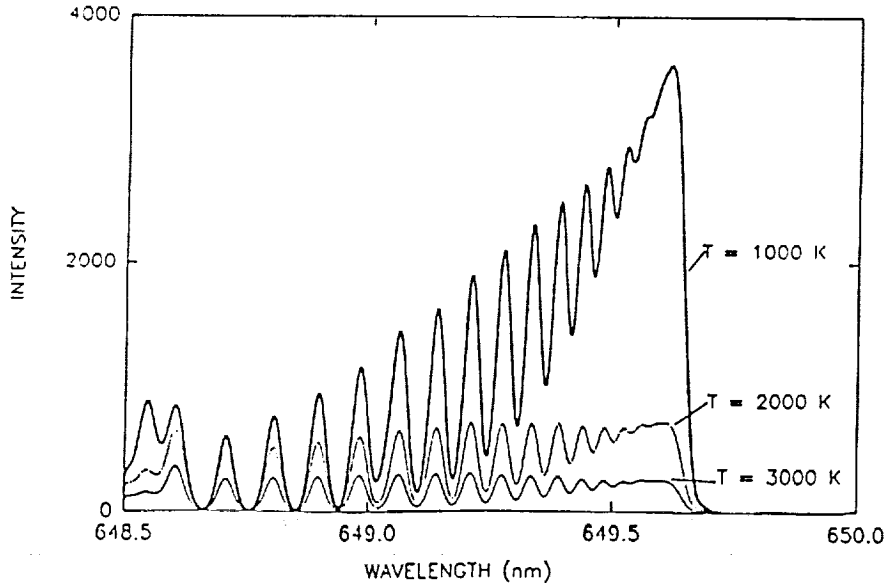

Figure 4. Predicted Raman Q-branch for oxygen at three different temperatures.

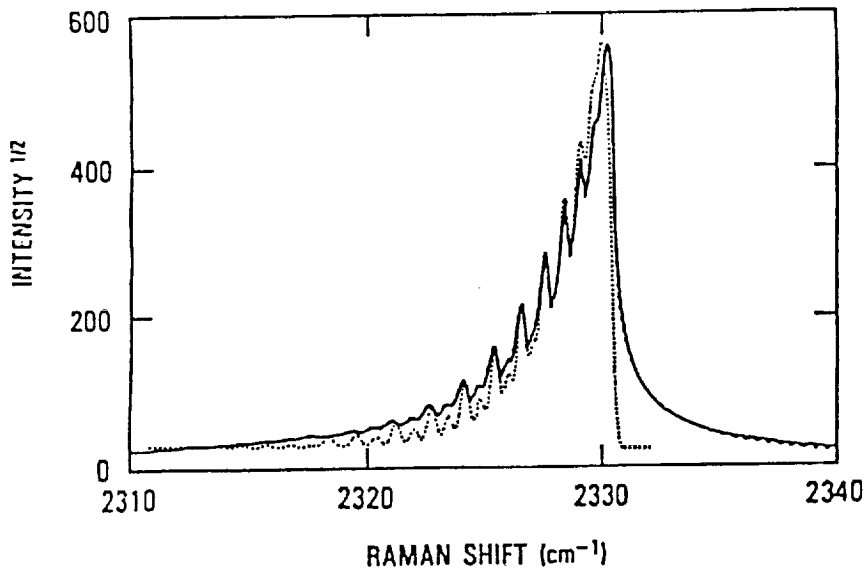

a. T = 298 K; P = 1 atm.

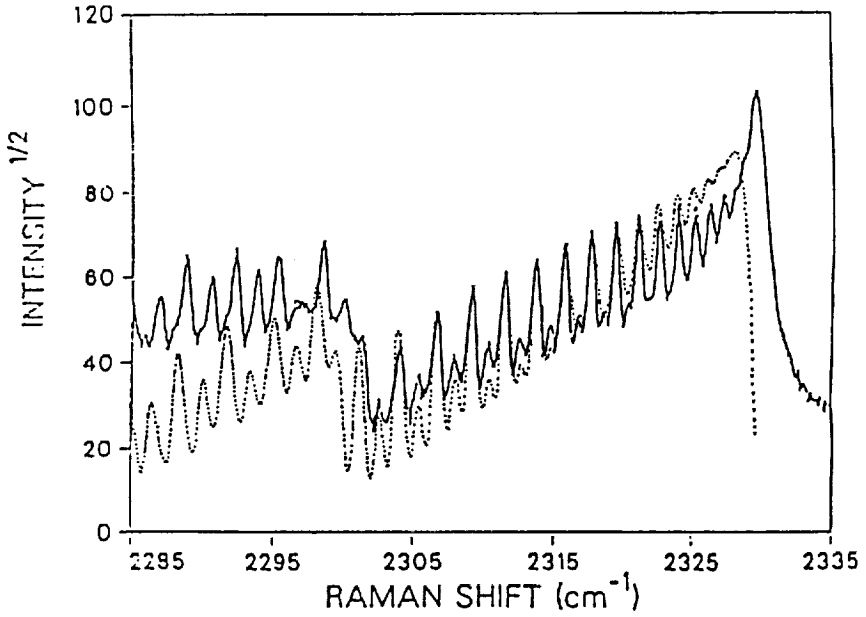

b. T = 2310 K; P = 16 atm.

Figure 5. Comparison of predicted (·····) and measured (Ref. 17) (——) Raman Q-branch of nitrogen for two different conditions.

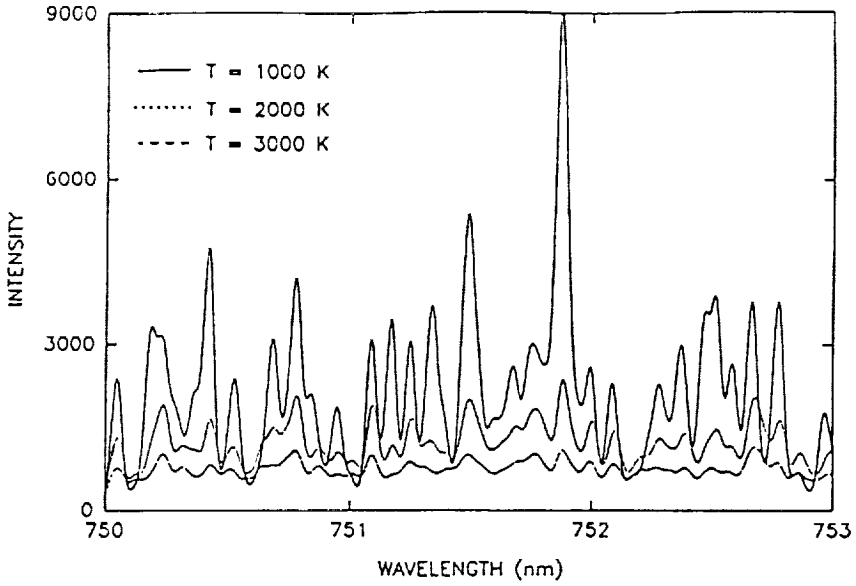

Figure 6. Predicted Raman spectrum of water at the Raman shift of the first vibration (ν_1) for three different temperatures.

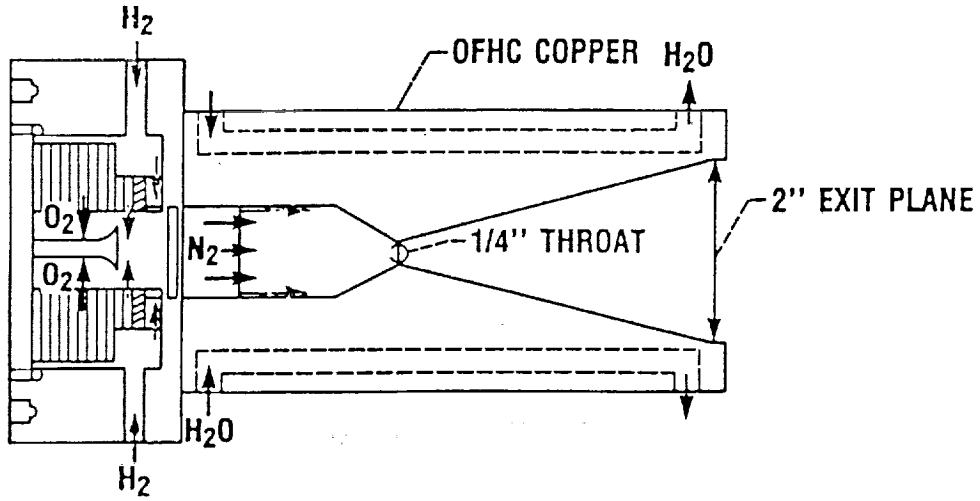

Figure 7. Two-dimensional test rocket.

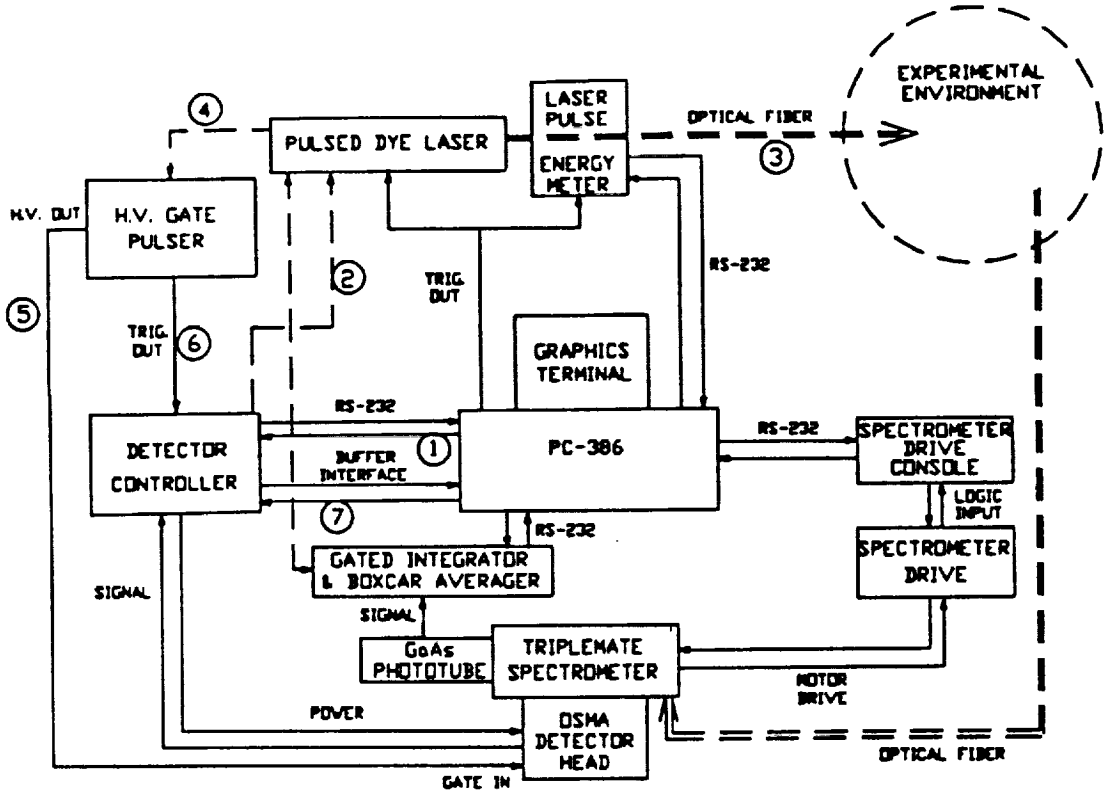

a. experimental schematic.

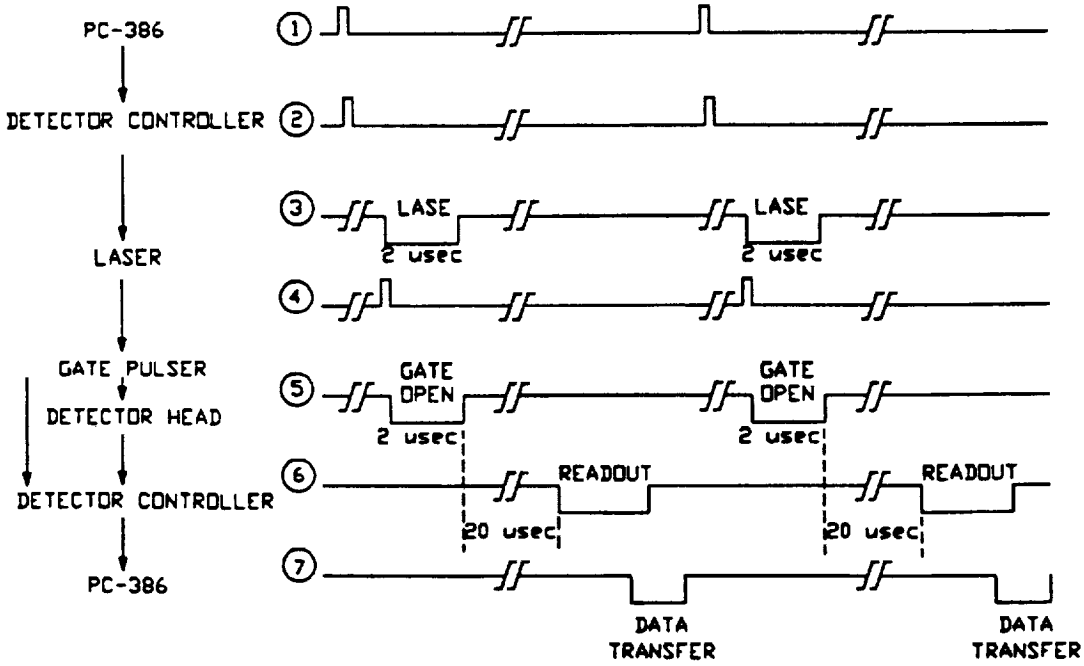

b. timing diagram.

Figure 8. Experimental schematic and timing diagram of Raman data acquisition system.

REPORT DOCUMENTATION PAGE

Form Approved
OMB No. 0704-0188

1. AGENCY USE ONLY (*Leave blank*)	2. REPORT DATE	3. REPORT TYPE AND DATES COVERED
	July 1992	Interim Contractor Report

4. TITLE AND SUBTITLE

The Development of a Fiber Optic Raman Temperature Measurement System for Rocket Flows

5. FUNDING NUMBERS

WU–506–42–31

6. AUTHOR(S)

Wim A. de Groot

7. PERFORMING ORGANIZATION NAME(S) AND ADDRESS(ES)

Sverdrup Technology, Inc.
Lewis Research Center Group
2001 Aerospace Parkway
Brook Park, Ohio 44142

8. PERFORMING ORGANIZATION REPORT NUMBER

E–7167

9. SPONSORING/MONITORING AGENCY NAMES(S) AND ADDRESS(ES)

National Aeronautics and Space Administration
Lewis Research Center
Cleveland, Ohio 44135–3191

10. SPONSORING/MONITORING AGENCY REPORT NUMBER

NASA CR–189200

11. SUPPLEMENTARY NOTES

Prepared for the 27th Joint Propulsion Conference and Exhibit cosponsored by the AIAA, SAE, ASME, and ASEE, June 24–27, 1991. Responsible person, Wim A. de Groot, (216) 433–7485.

12a. DISTRIBUTION/AVAILABILITY STATEMENT

Unclassified - Unlimited
Subject Categories 72 and 20

12b. DISTRIBUTION CODE

13. ABSTRACT ***(Maximum 200 words)***

A fiberoptic Raman diagnostic system for H_2/O_2 rocket flows is currently under development. This system is designed for measurements of temperature and major species concentration in the combustion chamber and part of the nozzle of a 100 Newton thrust rocket currently undergoing tests. This paper describes a measurement system based on the spontaneous Raman scattering phenomenon. An analysis of the principles behind the technique is given. Software is developed to measure temperature and major species concentration by comparing theoretical Raman scattering spectra with experimentally obtained spectra. Equipment selection and experimental approach are summarized. This experimental effort is part of a program, which is in progress, to evaluate Navier-Stokes based analyses for this class of rockets.

14. SUBJECT TERMS

Raman scattering; H_2/O_2 rockets

15. NUMBER OF PAGES

24

16. PRICE CODE

A03

17. SECURITY CLASSIFICATION OF REPORT	18. SECURITY CLASSIFICATION OF THIS PAGE	19. SECURITY CLASSIFICATION OF ABSTRACT	20. LIMITATION OF ABSTRACT
Unclassified	Unclassified	Unclassified	